LETTER

doi:10.1038/nature12644

A high-resolution map of the three-dimensional chromatin interactome in human cells

Fulai Jin[1]*, Yan Li[1]*, Jesse R. Dixon[1,2], Siddarth Selvaraj[1,3], Zhen Ye[1], Ah Young Lee[1], Chia-An Yen[1], Anthony D. Schmitt[1,4], Celso A. Espinoza[1] & Bing Ren[1,5]

A large number of *cis*-regulatory sequences have been annotated in the human genome[1,2], but defining their target genes remains a challenge[3]. One strategy is to identify the long-range looping interactions at these elements with the use of chromosome conformation capture (3C)-based techniques[4]. However, previous studies lack either the resolution or coverage to permit a whole-genome, unbiased view of chromatin interactions. Here we report a comprehensive chromatin interaction map generated in human fibroblasts using a genome-wide 3C analysis method (Hi-C)[5]. We determined over one million long-range chromatin interactions at 5–10-kb resolution, and uncovered general principles of chromatin organization at different types of genomic features. We also characterized the dynamics of promoter–enhancer contacts after TNF-α signalling in these cells. Unexpectedly, we found that TNF-α-responsive enhancers are already in contact with their target promoters before signalling. Such pre-existing chromatin looping, which also exists in other cell types with different extracellular signalling, is a strong predictor of gene induction. Our observations suggest that the three-dimensional chromatin landscape, once established in a particular cell type, is relatively stable and could influence the selection or activation of target genes by a ubiquitous transcription activator in a cell-specific manner.

We carried out Hi-C experiments to study the dynamic chromatin interactions in a primary human fibroblast cells (IMR90) in response to transient TNF-α signalling. Hi-C data from IMR90 cells before and after 1 h TNF-α treatment were combined, to produce a total of approximately 3.4 billion uniquely mapped paired-end reads from 6 biological replicates in each condition, among which approximately 1.4 billion are intra-chromosomal reads (Supplementary Tables 1 and 2). To accurately identify chromatin looping interactions with high sensitivity and resolution, we devised an improved data filtering strategy[6] based on the strand orientation of Hi-C paired-end reads (Supplementary Figs 1–6 and Supplementary Methods), which results in over 500 million high-confidence read pairs (Supplementary Tables 1 and 2), each representing a legitimate ligation event between two restriction fragments on the same chromosome. As we recognized that some reads may be due to random collision events between restriction fragments[4,7], we also estimated the expected frequency between any two restriction fragments, and then fitted a negative binomial model to assess the significance of observed contact frequency (Supplementary Methods and Supplementary Figs 7–9). Compared to previous methods[4], our data analysis method permits detection of chromatin interactions at short distance. For example, we observed asymmetric distribution of *cis*-contacts from highly expressed promoters to the immediate downstream gene bodies (Supplementary Fig. 10). This observation is reminiscent of a recent study showing interactions between a subset of exons and their promoters[8]. Interestingly, although such bias at promoters is correlated with elongation of RNA polymerase II, it remains when transcription elongation is blocked by the positive transcription elongation factor b (P-TEFb) inhibitor flavopiridol (Supplementary Fig. 11), suggesting that the maintenance of promoter–gene-body contacts is independent of active transcription.

To accurately map at high resolution the chromatin interactions genome-wide, we devised an algorithm (Supplementary Fig. 12) to identify statistically significant looping interactions centred on a given genomic region from Hi-C contact matrix (Fig. 1a). We applied this method to the *CCL2* (chemokine (C-C motif) ligand 2) locus, and were able to determine the distal enhancers and CTCF (a chromatin organizer) binding sites interacting with the *CCL2* promoter (Fig. 1a, b). Our algorithm also identified a number of previously reported long-range chromatin interactions at the homoebox A (*HoxA*) gene cluster[9] and the sonic hedgehog (*SHH*) locus[10], which were not readily observable from lower resolution analysis (Supplementary Figs 13 and 14). We then performed conventional 3C experiments to validate six pairs of long-range interactions identified at five different genes, and the results confirmed the reliability of our method (Fig. 1c and Supplementary Fig. 15).

We next applied the above algorithm to the 518,032 anchor regions in the human genome, with each containing one or a few HindIII restriction fragments (fragments shorter than 2 kilobases (kb) are merged) (Fig. 2a), and uncovered a total of 1,116,312 chromatin interactions with a false discovery rate (FDR) of 0.1 (Supplementary Data). We found that strong interactions supported by lower *P* values and higher contact frequencies are more reproducible between biological replicates (Supplementary Fig. 16). As interactions between loci separated by more than 2 megbases (Mb) are very rare (Fig. 2c), we limit our search to this genomic span. The sizes of the identified interacting DNA loci range from several hundred base pairs to over 50 kb, with a median of 10.5 kb (Fig. 2b). We were able to identify chromatin interactions that span a genomic distance from several hundred base pairs to over 1 million base pairs (Fig. 2c). Consistent with previous reports that the genome is partitioned into megabase-sized topological domains[11–13], we found that a majority of the identified chromatin interactions in the IMR90 cells are located within the same topological domains (Fig. 2d and Supplementary Fig. 18).

We next characterized the chromatin interactions centred on the *cis*-elements annotated in the IMR90 cell genome[14] (Supplementary Data). Chromatin looping interactions are significantly enriched at *cis*-regulatory elements, particularly active promoters, enhancers and CTCF binding sites, and are rare at inactive transcription start sites (TSSs) or regions with repressive chromatin domains marked by H3K27me3 (Fig. 2e, f)[15]; notably, both active and poised enhancers (distinguished be the status of H3K27ac)[16–18] are found equally likely to engage looping interactions (Fig. 2e, f), raising the possibility that DNA looping could take place after priming of enhancers by H3K4me1 but before further activation[19]. Interestingly, the chromatin interactions

[1]Ludwig Institute for Cancer Research, 9500 Gilman Drive, La Jolla, California 92093, USA. [2]UCSD Medical Scientist Training Program, University of California, San Diego, School of Medicine, 9500 Gilman Drive, La Jolla, California 92093, USA. [3]UCSD Bioinformatics and Systems Biology Graduate Program, University of California, San Diego, 9500 Gilman Drive, La Jolla, California 92093, USA. [4]UCSD Biomedical Sciences Graduate Program, University of California, San Diego, School of Medicine, 9500 Gilman Drive, La Jolla, California 92093, USA. [5]Department of Cellular and Molecular Medicine, Institute of Genome Medicine, Moores Cancer Center, University of California, San Diego, School of Medicine, 9500 Gilman Drive, La Jolla, California 92093, USA.
*These authors contributed equally to this work.

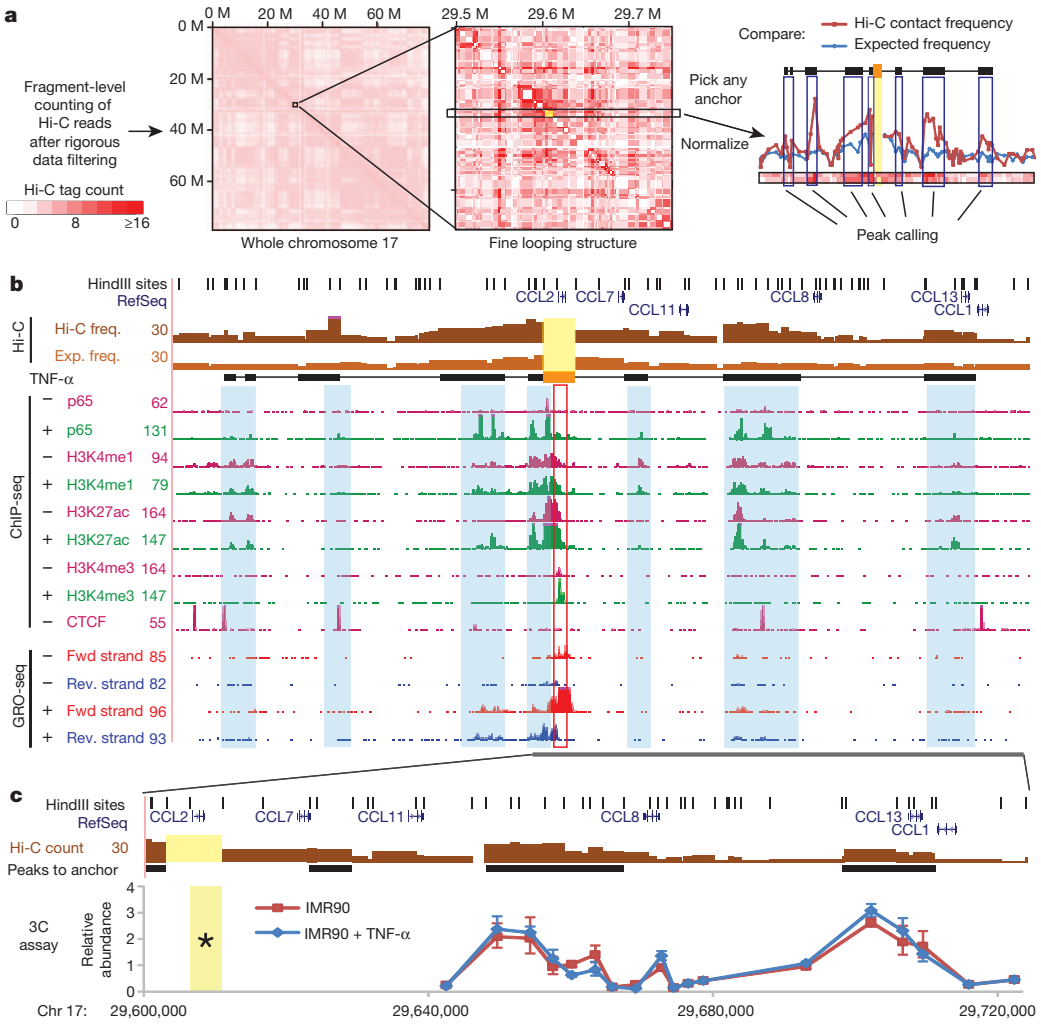

Figure 1 | Fine mapping of chromatin interactions in IMR90 cells. **a**, An illustration of the Hi-C data analysis procedure to identify regions interacting with a selected genomic region, such as the *CCL2* locus, highlighted in yellow (Supplementary Methods). **b**, Genome-browser shot of the *CCL2* locus showing the results from Hi-C, ChIP-seq and GRO-seq experiments. Each bar in the top two tracks are either Hi-C reads count (dark brown) or expected frequency (light brown) from a fragment to *CCL2* locus (highlighted in yellow and orange filled box). Black filled boxes are regions interacting with *CCL2* called by the peak calling algorithm same as the black filled boxes in **a**. Light blue shadows highlight the enhancer and CTCF locations from ChIP-seq data. Induction of *CCL2* by TNF-α is shown in the GRO-seq tracks. **c**, Validation of the DNA looping interactions with *CCL2* using 3C assays. Yellow, anchor fragments in Hi-C or 3C (asterisk). Error bar: s.d. from 3 technical replicates.

centred on CTCF binding sites tend to occur over a longer range than other types of *cis*-elements (Fig. 2g), confirming a recent result obtained from selected loci[20]. We also explored the spatial organization of *cis*-elements by examining preferential interaction between different classes of elements. Strongest enrichment was observed between H3K27me3 marked regions (Fig. 2h), consistent with the known compact three-dimensional structure at this type of repressive chromatin domains[21] (for example, Supplementary Fig. 14a). The inactive promoters tend to interact with regions depleted of enhancers but enriched for repressive mark H3K27me3 (Fig. 2h), whereas CTCF binding sites loop to both active and inactive promoters with no preference, as reported previously[15]. It is also interesting to observe that CTCF binding sites seem to prefer promoters over enhancers (Fig. 2h), suggesting a specific role for CTCF in organizing long-range chromatin interactions to promoters.

Looping interactions between *cis*-regulatory elements and gene promoters have been shown to be important for transcription regulation at a number of loci[3]. The genome-wide identification of chromatin interactions in the IMR90 cells allowed us to examine this concept systematically. We first focused on the looping interactions anchored to gene promoters, and denote the identified interacting sequences as promoter tethered regions (PTRs) (Fig. 3a). In IMR90 cells, we found 57,585 PTRs identifying 29,132 enhancer–promoter pairs involving 6,133 active promoters and 15,432 distal active enhancers (Supplementary Data). Only approximately 25% of enhancer–promoter pairs are within a 50-kb range, and approximately 57% span 100 kb or larger genomic distance, with a median distance of 124 kb (Fig. 3b). We assigned 55% of distal enhancers to at least one active promoter, and 25% of enhancers to two or more active promoters (Fig. 3c, left panel). This result confirms previous observation that promoters and enhancers often form complex networks to regulate transcription[15]. We further reasoned that genes sharing common enhancers (denoted hub enhancers) are likely to have coordinated gene expression patterns. Indeed, genes sharing the same nuclear factor κB (NF-κB)-responsive enhancers are more frequently induced together by TNF-α than expected by chance (Fig. 3d). As an example, *CKAP2L* and *IL1A* are induced simultaneously by TNF-α although lacking promoter-bound p65 peaks, and they share overlapping distal PTRs containing multiple NF-κB binding sites (Fig. 3e). Similar examples can be found in other gene clusters co-induced by TNF-α treatment (Supplementary Fig. 19). These results therefore provide a molecular mechanism for coordinated gene expression of neighbouring genes.

Interestingly, 46% of the active genes do not interact with any distal enhancer (Fig. 3c, right panel). Gene ontology analysis showed that these genes are enriched with housekeeping genes (Supplementary Fig. 20a). The remaining 54% of the active promoters demonstrate extensive looping interacting with enhancers (average 4.75 enhancers per gene, Fig. 3c, right panel), and they are enriched with genes related to biological pathways such as signal transduction (Supplementary Fig. 20b). This analysis suggests that housekeeping genes, despite being highly transcribed, do not engage a lot of distal regulatory elements. Conversely, genes involved in cell-specific functions are under extensive control of distal regulator sequences.

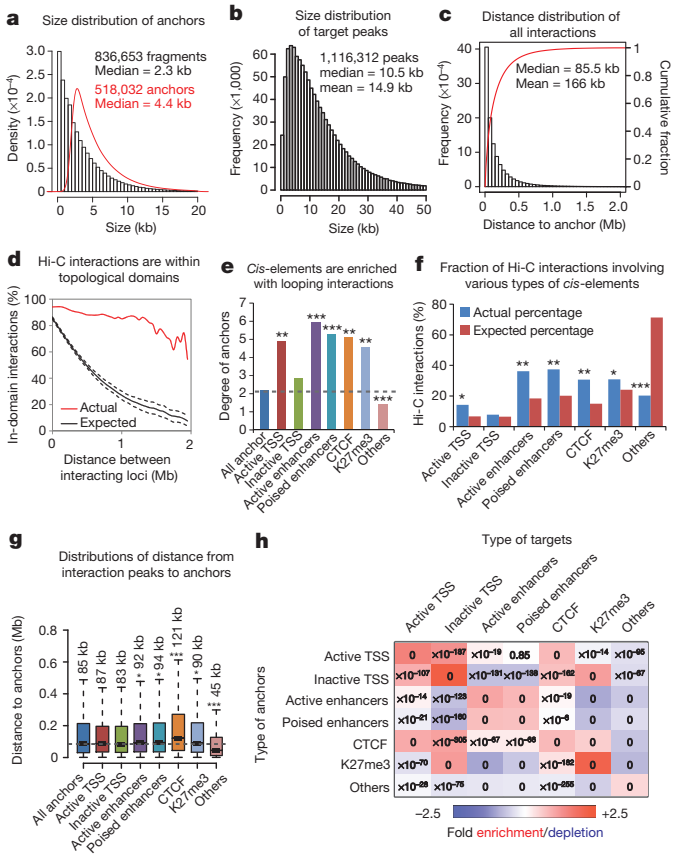

Figure 2 | Characterization of the IMR90 chromatin interactome. **a**, Histogram showing the size distribution of all HindIII restriction fragments in human genome. The red curve plots the size distribution of all anchors used in this study. **b**, Size distribution of the genomic regions identified as interacting with all anchors. **c**, Distribution of genomic spans of all identified chromatin interactions. Histogram, frequency distribution; red curve, cumulative fraction with increasing distances. **d**, Fraction of chromatin looping interactions that fall within the same topological domains is plotted as a function of genomic distance between the two interacting loci (red curve). Black curve, expected fraction calculated from random shuffling locations of topological domains (100 iterations; dashed error lines, s.d.). **e**, Average number of peaks identified for anchors with different *cis*-elements. **f**, Percentages of all interactions involving various types of *cis*-elements (either anchor or target peak has the elements). In **e** and **f**, *Z*-scores were calculated comparing the actual values to simulation by randomly shuffling the locations of *cis*-elements (100 iterations, two-side *Z*-test). $*Z > 50$, $**Z > 100$, $***Z > 150$. **g**, Box plot showing the distance distribution from different types of anchors to their targets. Median distances are also labelled. *t*-statistics are computed comparing log-transformed distance between each type of anchors to all anchors as control (dash horizontal line). $*t > 20$, $**t > 40$, $***t > 80$ (two-side *t*-test). **h**, Preferential interactions between different types of *cis*-elements. Heatmap shows the fold enrichment of different type of pair-wise combinations. *P* values are computed using hypergeometric test and denoted in each cell.

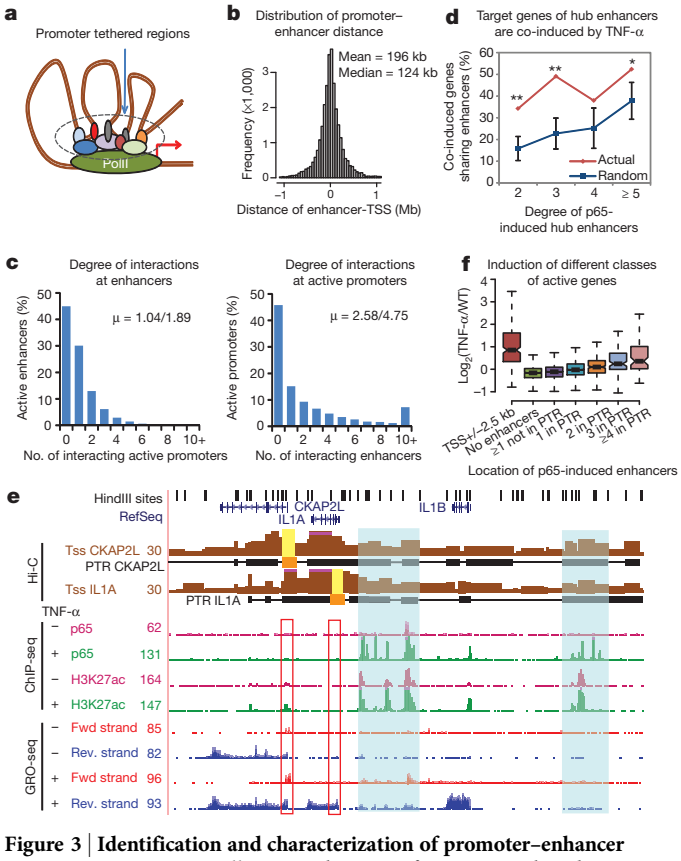

Figure 3 | Identification and characterization of promoter–enhancer interactions in IMR90 cells. **a**, A schematic of promoter tethered regions (PTRs). **b**, Distribution of distances between the promoters and enhancers found within the PTRs. **c**, Bar charts show the degrees of interactions. Left, percentage of enhancers that are looped to active promoters found in PTRs. The first value of μ is the mean degree of promoter interactions for all enhancers; the second value is the mean degree of promoter interactions for enhancers interacting with at least one promoter. Right, distribution of degrees of enhancer interactions for active promoters. **d**. Genes sharing enhancers are co-regulated. Among the target genes of TNF-α-responsive hub enhancers, proportion of co-induced gene pairs (greater than twofold) are plotted and compared to random simulation (100 iterations, two-side *Z*-test, $*P < 0.05$, $**P < 0.01$, error bar, s.d.). **e**, Genome browser snapshots showing the virtual 3C plots of the *CKAP2L* and *IL1A* promoters. **f**, Box plots comparing the induction of different gene groups based on the location of p65-induced enhancers. 'No enhancers', genes with no such enhancers within 2 Mb; '≥1 not in PTR', p65-induced enhancers are within 2 Mb but not in PTR.

We next examined long-range looping interactions at transcriptional enhancers, focusing on those bound by the p65 subunit of NF-κB transcription factor. Using chromatin immunoprecipitation followed by high-throughput sequencing (ChIP-seq), we identified 15,621 p65 binding sites in the genome after TNF-α treatment, 2,315 (14.8%) of which can be classified as 'active p65 binding sites' because they exhibit increased H3K27ac levels and enhancer RNA expression upon TNF-α signalling (Supplementary Figs 21 and 22). Consistent with their putative role in mediating transcriptional induction, these active p65 binding sites are enriched near TNF-α-dependent genes (Supplementary Fig. 22c). We next tested whether the long-range interactions between these p65 binding sites and their target promoters are correlated with transcriptional induction. Indeed, at the promoters that exhibit interactions with one or more active p65 binding sites, significantly higher levels of transcriptional induction were observed than the promoters that do not interact with distal p65 binding sites (Fig. 3f), suggesting that the identified long-range chromatin interactions may have a key role in transcriptional regulation of the TNF-α-inducible genes.

The high-resolution map of chromatin interactions may also improve the prediction of target genes of distal enhancers. Currently, a common practice is to assign distal enhancers to their nearest promoters, assuming one enhancer is linked to just one target gene (proximity approach). However, this approach cannot explain all of the 828 TNF-α-responsive genes. We found that 331 (40%) of these genes have one or more p65 binding sites within 2.5 kb of their promoters, and 362 genes of the remainder can be assigned to one or more NF-κB binding sites by proximity approach, leaving still 135 TNF-α-induced genes unexplained. Using a recently published enhancer–promoter connection map[22] based on correlated chromatin features across diverse tissues or cell types, we were able to link 10 of the 135 unexplained TNF-α-inducible genes to distal NF-κB binding sites. Using the chromatin interactome map, 74 (55%) of the unexplained genes can be assigned to a NF-κB binding site (Supplementary Fig. 23). This result illustrates that the chromatin

interactome map described here could be valuable for the study of long-range regulation of gene expression by transcription factors.

We found no obvious alterations of megabase topological domains[12] in IMR90 cells after TNF-α treatment (for example, Supplementary Fig. 13). As previous studies have shown that gene activation by enhancers is accompanied by alteration of chromatin interactions[3,23,24], we expected that at shorter distance, binding of NF-κB to enhancers would induce looping interactions that bring the distal enhancers to proximity with target genes. To our surprise, we found that at the vast majority of TNF-α responsive enhancers, there is little change of DNA looping after treatment (Fig. 4a). These results suggest that in general, enhancer–promoter interactions already form in untreated cells; and these pre-existing DNA-structures are not significantly altered by transient activation or repression of enhancers. 3C assays confirm that DNA looping exists at several loci before TNF-α treatment (Fig. 1e and Supplementary Fig. 15a–c). We further compared the normalized reads count anchored to the TNF-α-activated enhancers at different ranges of genomic distances (Fig. 4b and Supplementary Methods). Consistent with the results in Fig. 4a, transient activation of p65-bound enhancers does not lead to significant changes in chromatin interactions (Fig. 4b). By contrast, the chromatin interactions (especially within a short genomic distance) at cell-type-specific enhancers are highly variable between cell types (Fig. 4c, d), suggesting the existence of specific chromatin interaction structures at cell-type-specific enhancers. Interestingly, the discrepancy between signal-dependent and cell-type-specific enhancers is well correlated with the levels of H3K4me1 at those dynamically regulated enhancers: despite the quick induction of the H3K27ac mark at TNF-α-responsive enhancers, strength of H3K4me1 signal is largely unchanged (Fig. 4e), but on the other hand, cell-type-specific enhancers have highly cell-specific H3K4me1 occupancy (Fig. 4f).

Recently, pre-existing promoter–enhancer looping was observed at several loci induced by p53, FOXO3 and glucocorticoid receptor using the 4C (chromosome conformation capture combined with sequencing) approach[20,25,26]. Our genome-wide analysis of chromatin interactome maps in IMR90 cells suggests that this is likely to be a common rule rather than a special case. To further demonstrate its generality, we examined six additional promoter–enhancer pairs by 3C assays in four different cell types (IMR90, HUVEC, MCF7 and LNCaP cells) under different stimuli (IFN-γ, TNF-α, β-oestradiol and 5α-dihydrotestosterone, respectively). In all of these examples, we found evident pre-existing promoter–enhancer contacts, and the looping interactions are largely unchanged after enhancer activation and target gene induction (Supplementary Figs 15d and 24). Our results predict that pre-existing chromatin looping interactions could dictate the spectrum of the target genes for a transcription factor even before it is activated. Indeed, p65 binding sites looping to the promoters before induction are much more likely to result in transcriptional activation of the linked gene than otherwise (Fig. 4g). This trend is particularly obvious when the p65-binding sites are located far from the linked promoters. On the basis of this observation, we conclude that pre-existing DNA-looping interactions between enhancers and promoters allow a ubiquitous, signal-dependent transcription factor to affect a selected set of genes in a cell-type-specific manner.

In summary, we have demonstrated that enhancer–promoter interactions already form in each cell type before the binding of signal dependent transcription factors, and they undergo relatively few changes during transient transcriptional activation. Several recent genome-wide studies have revealed that in different cell types, the repertoire of specific enhancers provides a unique context for the activation of different transcriptional programs in response to signal-dependent transcription factors including NF-κB[19,27–30]. Here, our results further suggest that targets of cell-specific enhancers are already hardwired into the chromatin architecture in each cell lineage. We therefore propose that cell-type-specific looping structure, by controlling the accessibility of the enhancers to their specific targets, may form an additional layer of regulation in determining the distinct transcription programs in different cell types.

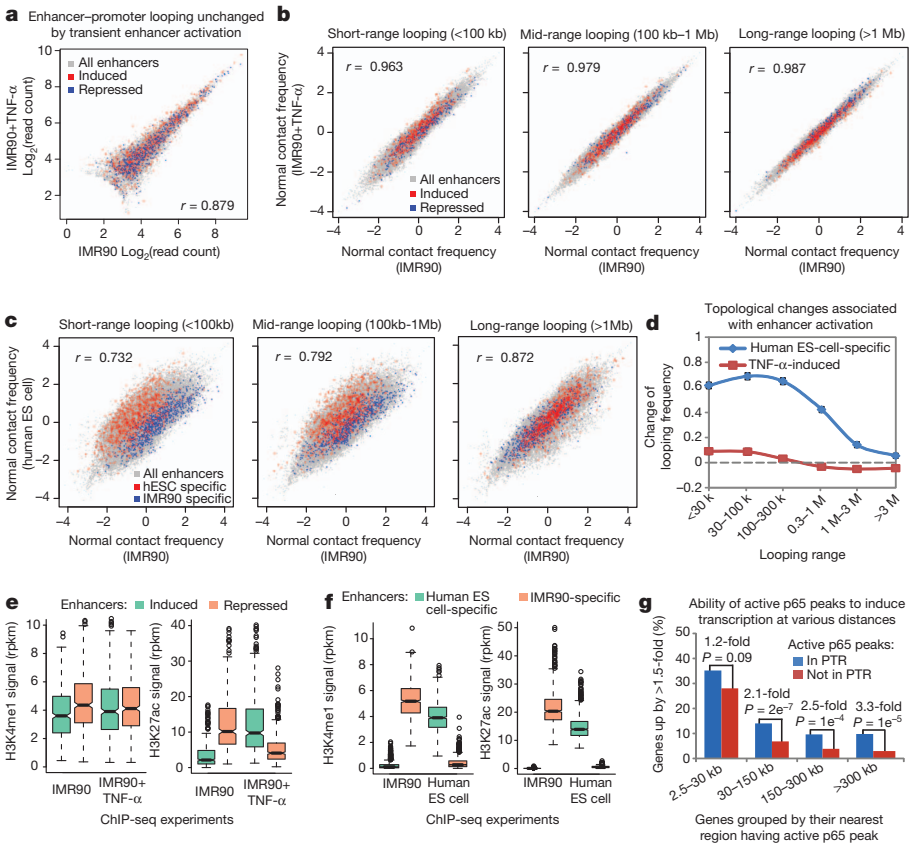

Figure 4 | The higher order chromatin structure in IMR90 cells is stable during transient TNF-α signalling. **a**, A scatter plot comparing reads count at PTRs before and after TNF-α treatment. Grey dots are data for PTRs involving all enhancers, red or blue dots are PTRs involving the top 500 induced or repressed enhancers, respectively. *r*, Pearson's correlation calculated from all data points. **b**, Scatter plots compare normalized contact frequencies (Supplementary Methods) of all enhancers before and after 1 h TNF-α stimulation. **c**, Scatter plots compare contact frequencies of enhancers in IMR90 and hESC cells. Coloured points represent the top 2,000 human embryonic stem cell (ES-cell)-specific (red) or IMR90-specific (blue) enhancers defined by H3K27ac mark. **d**, The relative change of contact frequency (comparing to untreated IMR90 cells) at human ES-cell-specific or TNF-α-induced enhancers are plotted in line graphs. **e**, Box plots of H3K4me1 and H3K27ac signals on enhancers that show increased or decreased H3K27ac signals after TNF-α treatment. rpkm, reads per kilobase per million. **f**, Boxplots of H3K4me1 and H3K27ac ChIP-seq signals at the IMR90- or hESC-specific enhancers. **g**, Bar charts showing that NF-κB binding sites within PTRs are more likely to activate target genes than those outside PTRs. In this figure, PTRs are identified using the Hi-C data from untreated IMR90 cells. The *P* values are calculated using hypergeometric test.

METHODS SUMMARY

Hi-C experiments were performed in human primary IMR90 fibroblasts. ChIP-seq, global run-on sequencing (GRO-seq), or RNA-seq libraries were also generated from IMR90, HUVEC, MCF7 or LNCaP cells and sequenced on the Illumina Hi-Seq2000 platform. All the reads were mapped to reference human genome (hg18). More information about the experiments and detailed descriptions of Hi-C data analysis pipeline, including data filtering, normalization, statistical modelling and interaction calling can be found in Supplementary Methods.

Received 30 December 2012; accepted 6 September 2013.
Published online 20 October 2013.

1. The ENCODE Project Consortium. An integrated encyclopedia of DNA elements in the human genome. *Nature* **489,** 57–74 (2012).
2. Maurano, M. T. *et al.* Systematic localization of common disease-associated variation in regulatory DNA. *Science* **337,** 1190–1195 (2012).
3. Smallwood, A. & Ren, B. Genome organization and long-range regulation of gene expression by enhancers. *Curr. Opin. Cell Biol.* **25,** 387–394 (2013).
4. Dekker, J., Marti-Renom, M. A. & Mirny, L. A. Exploring the three-dimensional organization of genomes: interpreting chromatin interaction data. *Nature Rev. Genet.* **14,** 390–403 (2013).
5. Lieberman-Aiden, E. *et al.* Comprehensive mapping of long-range interactions reveals folding principles of the human genome. *Science* **326,** 289–293 (2009).
6. Imakaev, M. *et al.* Iterative correction of Hi-C data reveals hallmarks of chromosome organization. *Nature Methods* **9,** 999–1003 (2012).
7. de Wit, E. & de Laat, W. A decade of 3C technologies: insights into nuclear organization. *Genes Dev.* **26,** 11–24 (2012).
8. Mercer, T. R. *et al.* DNase I-hypersensitive exons colocalize with promoters and distal regulatory elements. *Nature Genet.* **45,** 852–859 (2013).
9. Noordermeer, D. *et al.* The dynamic architecture of *Hox* gene clusters. *Science* **334,** 222–225 (2011).
10. Lettice, L. A. *et al.* Disruption of a long-range *cis*-acting regulator for *Shh* causes preaxial polydactyly. *Proc. Natl Acad. Sci. USA* **99,** 7548–7553 (2002).
11. Zhang, Y. *et al.* Spatial organization of the mouse genome and its role in recurrent chromosomal translocations. *Cell* **148,** 908–921 (2012).
12. Dixon, J. R. *et al.* Topological domains in mammalian genomes identified by analysis of chromatin interactions. *Nature* **485,** 376–380 (2012).
13. Sexton, T. *et al.* Three-dimensional folding and functional organization principles of the *Drosophila* genome. *Cell* **148,** 458–472 (2012).
14. Hawkins, R. D. *et al.* Distinct epigenomic landscapes of pluripotent and lineage-committed human cells. *Cell Stem Cell* **6,** 479–491 (2010).
15. Sanyal, A., Lajoie, B. R., Jain, G. & Dekker, J. The long-range interaction landscape of gene promoters. *Nature* **489,** 109–113 (2012).
16. Creyghton, M. P. *et al.* Histone H3K27ac separates active from poised enhancers and predicts developmental state. *Proc. Natl Acad. Sci. USA* **107,** 21931–21936 (2010).
17. Hawkins, R. D. *et al.* Dynamic chromatin states in human ES cells reveal potential regulatory sequences and genes involved in pluripotency. *Cell Res.* **21,** 1393–1409 (2011).
18. Rada-Iglesias, A. *et al.* A unique chromatin signature uncovers early developmental enhancers in humans. *Nature* **470,** 279–283 (2011).
19. Heinz, S. *et al.* Simple combinations of lineage-determining transcription factors prime *cis*-regulatory elements required for macrophage and B cell identities. *Mol. Cell* **38,** 576–589 (2010).
20. Phillips-Cremins, J. E. *et al.* Architectural protein subclasses shape 3D organization of genomes during lineage commitment. *Cell* **153,** 1281–1295 (2013).
21. Francis, N. J., Kingston, R. E. & Woodcock, C. L. Chromatin compaction by a polycomb group protein complex. *Science* **306,** 1574–1577 (2004).
22. Thurman, R. E. *et al.* The accessible chromatin landscape of the human genome. *Nature* **489,** 75–82 (2012).
23. Ong, C. T. & Corces, V. G. Enhancer function: new insights into the regulation of tissue-specific gene expression. *Nature Rev. Genet.* **12,** 283–293 (2011).
24. Schoenfelder, S., Clay, I. & Fraser, P. The transcriptional interactome: gene expression in 3D. *Curr. Opin. Genet. Dev.* **20,** 127–133 (2010).
25. Melo, C. A. *et al.* eRNAs are required for p53-dependent enhancer activity and gene transcription. *Mol. Cell* **49,** 524–535 (2013).
26. Tan, P. Y. *et al.* Integration of regulatory networks by NKX3–1 promotes androgen-dependent prostate cancer survival. *Mol. Cell. Biol.* **32,** 399–414 (2012).
27. Jin, F., Li, Y., Ren, B. & Natarajan, R. P. U. 1 and C/EBP(alpha) synergistically program distinct response to NF-κB activation through establishing monocyte specific enhancers. *Proc. Natl Acad. Sci. USA* **108,** 5290–5295 (2011).
28. John, S. *et al.* Chromatin accessibility pre-determines glucocorticoid receptor binding patterns. *Nature Genet.* **43,** 264–268 (2011).
29. Mullen, A. C. *et al.* Master transcription factors determine cell-type-specific responses to TGF-beta signaling. *Cell* **147,** 565–576 (2011).
30. Jin, F., Li, Y., Ren, B. & Natarajan, R. Enhancers: multi-dimensional signal integrators. *Transcription* **2,** 226–230 (2011).

Supplementary Information is available in the online version of the paper.

Acknowledgements We thank C. K. Glass for sharing the GRO-seq protocol, and S. Kuan and L. Edsall for assistance with high-throughput DNA sequencing and the initial processing. This work is supported by funds from the Ludwig Institute for Cancer Research, the California Institute of Regenerative Medicine (RN2-00905) and US National Institutes of Health (P50 GM085764-03 and U01 ES017166).

Author Contributions Y.L., F.J. and B.R. designed the studies. Y.L. conducted most of the experiments; F.J. carried out the data analysis; J.R.D., Z.Y., A.Y.L., C.Y., A.D.S. and C.E. contributed to the experiments; S.S. contributed to the data analysis; F.J., Y.L. and B.R. prepared the manuscript.

Author Information All sequencing data described in this study have been deposited to GEO under the accession number GSE43070. Some sequencing data used in this study were previously published and accession numbers can be found in Supplementary Methods. All chromatin interactions called in IMR90 cells can be found in Supplementary Data. Reprints and permissions information is available at www.nature.com/reprints. The authors declare no competing financial interests. Readers are welcome to comment on the online version of the paper. Correspondence and requests for materials should be addressed to B.R. (biren@ucsd.edu).